ION CHANNELS, RECEPTORS AND TRANSPORTERS

Neutralisation of a single voltage sensor affects gating determinants in all four pore-forming S6 segments of $Ca_V1.2$: a cooperative gating model

**Stanislav Beyl · Katrin Depil · Annette Hohaus ·
Anna Stary-Weinzinger · Tobias Linder · Eugen Timin ·
Steffen Hering**

Abstract Voltage sensors trigger the closed–open transitions in the pore of voltage-gated ion channels. To probe the transmission of voltage sensor signalling to the channel pore of $Ca_V1.2$, we investigated how elimination of positive charges in the S4 segments (charged residues were replaced by neutral glutamine) modulates gating perturbations induced by mutations in pore-lining S6 segments. Neutralisation of all positively charged residues in IIS4 produced a functional channel ($IIS4_N$), while replacement of the charged residues in IS4, IIIS4 and IVS4 segments resulted in nonfunctional channels. The $IIS4_N$ channel displayed activation kinetics similar to wild type. Mutations in a highly conserved structure motif on S6 segments ("GAGA ring": G432W in IS6, A780T in IIS6, G1193T in IIIS6 and A1503G in IVS6) induce strong left-shifted activation curves and decelerated channel deactivation kinetics. When $IIS4_N$ was combined with these mutations, the activation curves were shifted back towards wild type and current kinetics were accelerated. In contrast, 12 other mutations adjacent to the GAGA ring in IS6–IVS6, which also affect activation gating, were not rescued by $IIS4_N$. Thus, the rescue of gating distortions in segments IS6–IVS6 by $IIS4_N$ is highly position-specific. Thermodynamic cycle analysis supports the hypothesis that IIS4 is energetically coupled with the distantly located GAGA residues. We speculate that conformational changes caused by neutralisation of IIS4 are not restricted to domain II (IIS6) but are transmitted to gating structures in domains I, III and IV via the GAGA ring.

S. Beyl · K. Depil · A. Hohaus · A. Stary-Weinzinger · T. Linder ·
E. Timin · S. Hering (✉)
Department of Pharmacology and Toxicology,
University of Vienna,
Althanstrasse 14,
1090 Vienna, Austria
e-mail: steffen.hering@univie.ac.at

Introduction

The entry of Ca^{2+} through voltage-gated Ca^{2+} channels has direct effects on muscle contraction, release of hormones and neurotransmitters, hearing, vision, gene expression and other important physiological functions [8]. L-type Ca^{2+} channel dysfunction can result from structural aberrations within their pore-forming α_1-subunits causing hypokalemic periodic paralysis and malignant hyperthermia sensitivity ($Ca_V1.1$), Timothy syndrome ($Ca_V1.2$), sinoatrial node function and hearing ($Ca_V1.3$) and incomplete congenital stationary night blindness ($Ca_V1.4$) [46].

The pore-forming α_1-subunits of voltage-gated Ca^{2+} channels are composed of four homologous domains formed by six transmembrane segments (S1–S6) that are linked together on a single polypeptide [6]. The voltage-sensing machinery is formed by multiple charged amino acids located in segment S4 and adjacent structures of each domain. Segments S6 of each domain form the conducting pore of the channel.

Hodgkin and Huxley [19] hypothesised that activation of voltage-gated ion channels is initiated by movement of charged particles across the membrane. This charge movement (called "gating current") was later directly measured for sodium channels [1]. Crystal structures of ion channels revealed that four domains in Na_V or in K_V comprise six transmembrane segments (S1–S6) that are assembled in such a way that S1–S4 form the voltage-sensing module and the remaining S5 and S6 segments form the ion-conducting pore

[26, 29]. In principle, the voltage-sensing and ion-conducting modules can function independently of one another [26]: voltage sensors can exist without ion pores [27, 32, 36] and two-transmembrane-segment channels (two TM) function without voltage sensors [7].

Gating-sensitive positions in the pore of Ca_V have been identified through extensive site-directed mutagenesis studies [20, 24, 34, 35, 50, 57]. Changes in stability of the open and/or closed states induced by pore mutations [29, 55, 56] or e.g. Zn^{2+} bridges constraining the S4 movement [31] are manifested in shifts of the activation curve and accompanying deceleration of deactivation kinetics. Interestingly, such gating distortions are characteristic of a CACNA1F mutation identified in an X-linked retinal disorder [16] and the Timothy syndrome [10, 42, 43].

Biophysical models describe voltage sensor movements and pore opening in K_V as separate transitions [4, 21, 25, 39, 51]. Based on these assumptions, the kinetic properties of mutants with gating disturbances in pore-forming S6 segments of Na_V (e.g. NaChBac [55, 56]) and Ca_V [2] have successfully been quantified.

The opening of the Shaker K_V channel involves multiple activation steps as the S4 segments move from the resting state towards the activated state, which is followed by a concerted opening transition of the S6 gate. This concept of Ledwell and Aldrich [25] is supported by biophysical studies in Shaker K_V [5, 9, 14, 22, 25, 28, 37–41, 45, 47, 52, 53].

Surprisingly, in a concatenated Shaker K_V, a single voltage sensor is sufficient to open and close the channel [13]. Furthermore, a recent molecular dynamics simulation of a potassium channel revealed that the downward movement of a single S4 segment can initiate channel closure [23]. Thus, if channel closure is a concerted movement of all four S6 gates then one S4 segment either directly or allosterically controls gating structures in all four domains.

Previously, a number of strong activation determinants were identified in pore-forming segments S6 of $Ca_V1.2$ [10, 20, 24]. In order to get insights into the link between the voltage-sensing S4 segments and pore residues of $Ca_V1.2$, we combined these pore mutations in all four S6 segments with a voltage-sensing S4 segment where the charged residues were replaced by neutral glutamines. Our results suggest that conformational changes in a single S4 segment (IIS4) are transmitted to specific residues (GAGA ring [10]) in all four pore-forming S6 segments.

Materials and methods

Mutagenesis Substitutions in S4 and S6 segments of the $Ca_V1.2$ α_1-subunit (GenBank™ X15539) were introduced using the QuikChange® Lightning Site-Directed Mutagenesis Kit (Stratagene) with mutagenic primers according to the manufacturer's instructions. All constructs were checked by restriction site mapping and sequencing.

Cell culture and transient transfection Human embryonic kidney tsA-201 cells were grown at 5 % CO_2 and 37 °C to 80 % confluence in Dulbecco's modified Eagle's/F-12 medium supplemented with 10 % (v/v) foetal calf serum and 100 units/ml penicillin/streptomycin. Cells were split with trypsin/EDTA and plated on 35 mm Petri dishes (Falcon) at 30–50 % confluence ~16 h before transfection. Subsequently, tsA-201 cells were co-transfected with cDNAs encoding wild type or mutant $Ca_V1.2$ α_1-subunits with auxiliary β_{2a} [30] as well as α_2-δ_1 [11] subunits and GFP to identify transfected cells.

The transfection of tsA-201 cells was performed using the FUGENE6 Transfection Reagent (Roche) following standard protocols. tsA-201 cells were used until passage number 15. No variation in channel gating related to different cell passage numbers was observed.

Ionic current recordings and data acquisition Barium currents (I_{Ba}) through voltage-gated Ca^{2+} channels were recorded at 22–25 °C by patch-clamping [15] using an Axopatch 200A patch clamp amplifier (Axon Instruments, Foster City) 36–48 h after transfection. The extracellular bath solution (in millimolars: $BaCl_2$ 5, $MgCl_2$ 1, HEPES 10 and choline-Cl 140) was titrated to pH 7.4 with methanesulphonic acid. Patch pipettes with resistances of 1 to 4 MΩ were made from borosilicate glass (Clark Electromedical Instruments, UK) and filled with pipette solution (in millimolars: CsCl 145, $MgCl_2$ 3, HEPES 10 and EGTA 10), titrated to pH 7.25 with CsOH. All data were digitised using a DIGIDATA 1200 interface (Axon Instruments, Foster City), smoothed by means of a four-pole Bessel filter and saved to disc. One hundred-millisecond current traces were sampled at 10 kHz and filtered at 5 kHz; tail currents were sampled at 50 kHz and filtered at 10 kHz. Leak currents were subtracted digitally using average values of scaled leakage currents elicited by a 10-mV hyperpolarizing pulse or electronically by means of an Axopatch 200 amplifier (Axon Instruments, Foster City). Series resistance and offset voltage were routinely compensated for. The pClamp software package (Version 7.0 Axon Instruments, Inc.) was used for data acquisition and preliminary analysis. Microcal Origin 7.0 was used for analysis and curve fitting.

The voltage dependence of activation was determined from I to V curves and fitted to

$$m_\infty = \frac{1}{1 + \exp\frac{V_{0.5,act} - V}{k_{act}}}$$

The time courses of current activation and deactivation were fitted to a mono-exponential function:

$I(t) = A \cdot \exp(\frac{t}{\tau}) + C$; where $I(t)$ is current at time t, A is the amplitude coefficient, τ is the time constant, and C the steady-state current. Data are given as mean±S.E. Time constants were plotted versus voltage (e.g. Fig. 1c). The left branch of the bell-shaped curve of the time constants corresponds to channel deactivation and the right branch to the activation (see [19]). At voltages where channel activation and deactivation overlap (peak of the bell-shaped dependence), the data are given as averaged values of both time constants.

Structural changes (point mutations) in Ca^{2+} channels may influence activation and inactivation properties (e.g. [10, 20, 24, 49]). To minimise effects of inactivation on the estimation of the rate of channel activation and deactivation, the α_1 subunit of $Ca_V1.2$ was co-expressed with the auxiliary β_{2a} subunit known to substantially slow the inactivation kinetics [17]. Furthermore, in order to remove Ca^{2+}-dependent inactivation, the experiments were performed with Ba^{2+} as charge carrier.

Modelling The homology model of $Ca_V1.2$ is based on the Na_VAb crystal structure [29] (protein databank identifier: 3RVY). Modeller 9v7 [12] was used to generate the model. Modelling criteria have been published previously [44].

Results

Charge neutralisation in IIS4 induces only small gating disturbances in $Ca_V1.2$

The location of the arginine and lysine residues (which we refer to as R1–R5) in the S4 segments is shown in Fig. 1a, b. We will use the designation S4$_N$ for a mutant with a "charge-neutralised" S4 segment in which all the positions R1–R5 are replaced by glutamines. Currents were measurable only through construct IIS4$_N$ (Table 1), while mutants IS4$_N$, IIIS4$_N$ and IVS4$_N$ did not result in expression of channels that conducted barium currents. This finding can either be explained by insufficient trafficking of the constructs to the membrane or by an impaired function of the channels. Applying a more negative holding potential (−140 mV) had no effect suggesting that these constructs are not in an inactivated state.

Channel gating of IIS4$_N$ was quite similar to the wild type (wt); no significant shift in the activation curve was observed ($\Delta V = 1.2 \pm 1.2$ mV, Fig. 1). At first glance, these results suggest that one or more of the other segments (IS4, IIIS4 and IVS4) play a role in voltage-dependent gating, while IIS4 has only a minor impact. However, combining IIS4$_N$ with mutations in S6 segments revealed that it had a significant impact on channel activation.

Charge neutralisation in segment IIS4 rescues gating disturbances in the GAGA ring in segments IS6–IVS6

First, we combined IIS4$_N$ with perturbing pore mutations in a highly conserved structure motif ("GAGA ring" [10]) of small residues in homologous positions of all four domains (Gly-432 (IS6), Ala-780 (IIS6), Gly-1193 (IIIS6) and Ala-1503 (IVS6)). All of these mutations have been shown to shift the activation curve to the left and to decelerate deactivation (see also [2, 20, 24, 35, 48]). For example, mutant G432W activates and deactivates (Fig. 2a, c, d) with the slowest activation/deactivation time constant of about 18 ms observed at −50 mV (Fig. 2d). However, gating disturbances induced by G432W in IS6 were "rescued" by combination with IIS4$_N$. In G432W/IIS4$_N$, the shift of the activation curve compared to wild type ($\Delta V = V_{0.5,mut} - V_{0.5,wt}$) was eliminated ($\Delta V = -0.5 \pm 1.1$ mV (G432W/IIS4$_N$) vs. -14.9 ± 1.0 mV (G432W), Fig. 2) and current kinetics were correspondingly faster with a maximal activation/deactivation time constant of about 5 ms at −20 mV (Fig. 2a, c, d). A similar result was obtained with G432N, shifting the activation curve to the left. Combining G432N with IIS4$_N$ reversed this shift ($\Delta V = -3.3 \pm 1.1$ mV (G432N/IIS4$_N$) vs. by 17.9 ± 1.1 mV (G432N)) and also accelerated deactivation (see Supplemental Fig. 1). Comparable rescue effects on gating disturbances were observed for constructs G1193T/IIS4$_N$ and A1503G/IIS4$_N$. Substantial shifts in channel activation ($\Delta V = -31.0 \pm 1.3$ mV in G1193T and -22.6 ± 1.2 mV in A1503G) were reduced to -2.0 ± 1.1 mV and -1.0 ± 1.1 mV in G1193T/IIS4$_N$ and A1503G/IIS4$_N$, respectively (coloured bars in Fig. 3b, Table 1). Current kinetics were also considerably faster; the maximal (slowest) time constants of current activation and deactivation for these constructs are given as coloured columns in Fig. 3c.

Interestingly, combining IIS4$_N$ with the gating disturbing A780T in IIS6 (a pore mutation in its "own" domain II) shifted the activation curve only partially towards wild type ($\Delta V = -25.2 \pm 1.1$ mV (A780T) vs. $\Delta V = -13.2 \pm 1.1$ mV in A780T/IIS4$_N$), without inducing significant changes in current kinetics (see shifts of the voltage dependence in Fig. 4c, d).

Charge neutralisation in IIS4 does not affect gating disturbances in positions neighbouring to GAGA

Mutations of residues upstream and downstream of the GAGA positions in segments IS6, IIIS6 and IVS6 (G432, G1193 and A1503, see alignment in Fig. 3a) resulted in a wide spectrum of gating phenotypes. Gating disturbances induced either leftward or rightward shifts of the activation curve (ranging from -28.3 ± 1.2 mV (I781T) to $+26.9 \pm 1.2$ mV (L431P)). None of these mutants was, however, sensitive to combination with IIS4$_N$. This is evident from Fig. 3 illustrating the steady-state activation (Fig. 3b) and the maximal time constants (Fig. 3c). Neither the
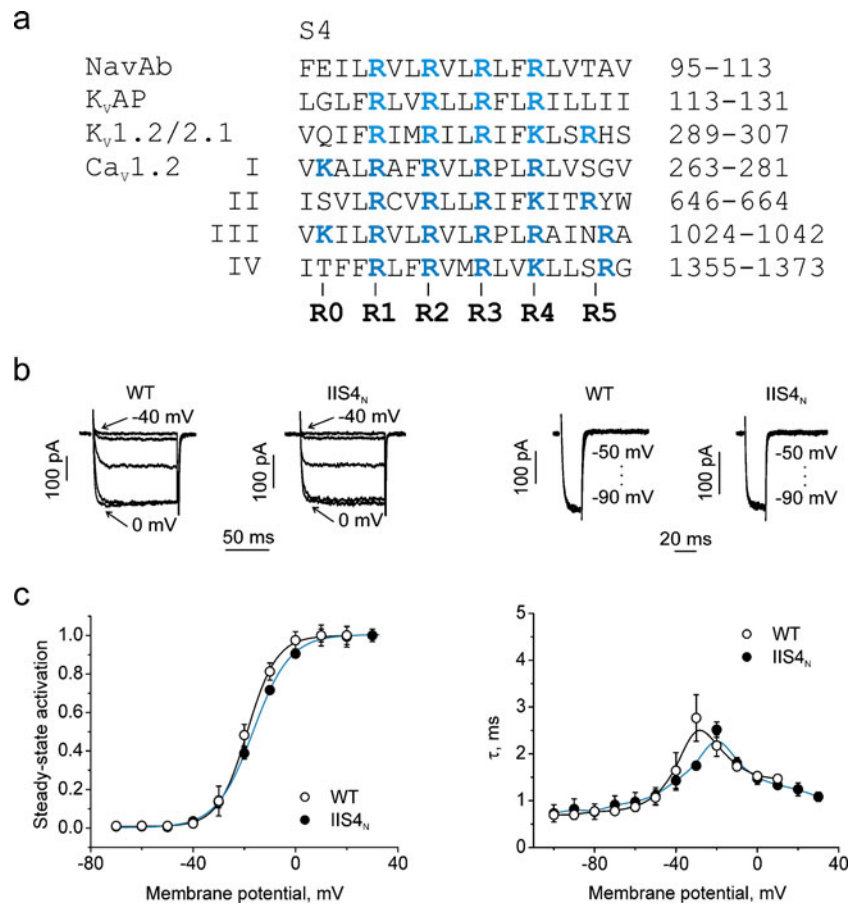
Fig. 1 Charge neutralisation in segment IIS4 of $Ca_V1.2$ has minor effects on activation gating: **a** alignment of S4 segments of Na_VAb (protein databank identifier, 3RVY), K_VAP (protein data bank identifier, 1ORS), $K_V1.2/2.1$ (protein data bank identifier, 2R9R) and $Ca_V1.2$ (accession number, P15381). Charged residues are shown in *blue*. **b** *Left panel* shows representative families of I_{Ba} through wild type channel and through the channel with the "charge-neutralised" IIS4 segment ($IIS4_N$). Barium currents were evoked during depolarization starting from −40 with 10 mV increments from a holding potential of −100 mV. *Right panel* shows representative tail currents. Currents were activated during a 20-ms conditioning depolarization to 0 mV. Deactivation was recorded during subsequent repolarisations with 10 mV increments starting from −100 mV. **c** *Left panel*, averaged activation curves of wild type ($n=9$) and $IIS4_N$ ($n=11$) channels. *Right panel*, voltage-dependent time constants of channel activation/deactivation

shifts of the activation curves nor the maximal time constants of the activation/deactivation were reversed towards wild type kinetics.

Charge neutralisation in segment IIS4 modulates kinetics of IIS6 pore mutants

That $IIS4_N$ only partially rescued gating disturbances induced by A780T is not unexpected. If a hyperpolarisation-driven downward movement of IIS4 initiates pore closure by moving IIS6 towards its closed position, then replacement of the charged arginines would inevitably decelerate the gate movement (channel closure) in domain II.

In line with such a scenario, constructs I781T/$IIS4_N$ and A782P/$IIS4_N$ displayed additional shifts of the activation curves compared to I781T and A782P. In I781T, ΔV amounted -28.3 ± 1.2 mV while charge neutralisation (I781T/$IIS4_N$) further increased ΔV to -36.0 ± 1.1 mV

(Fig. 4a, c middle column). Likewise, the shift of the activation curve in A782P/$IIS4_N$ ($\Delta V=-31.4\pm1.2$ mV) was also not rescued but increased compared to A782P (-24.2 ± 1.2 mV, Fig. 4a, c right column).

Interestingly, charge neutralisation in IIS4 decelerated deactivation of both constructs at negative voltages (from −60 to −100 mV), with little effect on kinetics of channel activation (from −40 to +30 mV). In L779P/$IIS4_N$, the leftward shift of the activation curve was less affected by charge neutralisation compared to the L779P ($\Delta V=-13.3\pm1.7$ mV (L779P/$IIS4_N$) vs. -12.4 ± 1.2 mV (L779P), Table 1) suggesting that this residue does not interact with IIS4.

Mutant cycle analysis reveals energetic coupling between IIS4 and residues of the GAGA ring

The position-specific effects of S4 neutralisation in domain II on gating perturbations in distant S6 segments were

Table 1 Midpoints and slope factors (k) of the activation curves and free energy changes during channel opening (ΔG, $\Delta\Delta G = \Delta G_{mut/IIS4n} - \Delta G_{IIS4n} - \Delta G_{mut}$)

Mutant	$V_{0.5}$, mV	k, mV	ΔG, kcal/mol	$\Delta\Delta G$, kcal/mol
wt	−18.8±0.9 (n=9)	5.7±0.9		
R1Q/R2Q/R3Q/R4Q/R5Q (IIS4$_N$)[a]	−17.5±0.8 (11)	6.7±0.7	0.39±0.36	
GAGA mutations				
G432W[b]	−33.7±0.6 (8)	4.7±0.4	−2.25±0.48	
G432N	−36.7±0.6 (6)	6.1±0.5	−1.58±0.43	
A780T[b]	−44.0±0.6 (5)	5.1±0.6	−3.10±0.67	
G1193T[c]	−49.8±1.0 (7)	5.1±0.6	−3.76±0.74	
A1503G[b]	−41.4±0.8 (5)	5.8±0.5	−2.23±0.48	
G432W/IIS4$_N$	−19.3±0.7 (8)	5.8±0.7	−0.01±0.40	1.84±0.72*
G432N/IIS4$_N$	−22.1±0.7 (6)	7.7±0.5	0.24±0.33	1.43±0.65 *
A780T/IIS4$_N$	−32.0±0.7 (10)	5.1±0.7	−1.73±0.64	0.96±0.99
G1193T/IIS4$_N$	−20.8±0.7 (5)	7.5±0.6	0.32±0.35	3.68±0.90*
A1503G/IIS4$_N$	−19.8±0.7 (6)	7.5±0.7	0.38±0.35	2.22±0.70*
GAGA−1 mutations				
L431P	8.1±0.7 (5)	7.4±1.0	2.56±0.33	
L431V	−8.4±1.3 (4)	6.7±0.8	1.19±0.34	
L779P	−31.2±0.8 (6)	6.1±0.6	−1.02±0.45	
V1192P	−13.8±0.7 (5)	6.6±1.0	0.70±0.37	
V1502P	−3.6±0.7 (6)	5.4±0.6	1.52±0.32	
L431P/IIS4$_N$	No measurable currents observed			
L431V/IIS4$_N$	−10.1±0.9 (4)	7.7±0.6	1.15±0.33	−0.43±0.60
L779P/IIS4$_N$	−32.1±1.5 (5)	5.4±1.6	−1.50±1.06	−0.87±1.21
V1192P/IIS4$_N$	−13.0±1.0 (5)	5.5±1.1	0.56±0.42	−0.53±0.67
V1502P/IIS4$_N$	−5.4±1.0 (7)	6.6±1.0	1.44±0.33	−0.48±0.59
GAGA+1 mutations				
V433C	−8.2±0.8 (5)	5.0±0.6	0.96±0.35	
V433L	−30.1±0.6 (5)	6.1±0.5	−0.95±0.39	
I781T	−47.1±0.9 (5)	7.4±0.7	−1.75±0.48	
F1194C	−6.8±0.9 (5)	4.4±0.6	1.02±0.36	
V1504T	−11.6±0.7 (7)	4.9±0.6	0.55±0.36	
V433C/IIS4$_N$	−12.4±0.7 (7)	5.7±0.6	0.65±0.35	−0.70±0.62
V433L/IIS4$_N$	−31.1±1.0 (4)	5.7 ±0.6	−1.25±0.47	−0.70±0.71
I781T/IIS4$_N$	−54.8±0.6 (9)	6.7±0.4	−2.79±0.42	−1.44±0.74*
F1194C/IIS4$_N$	−5.7±0.9 (5)	5.6±0.6	1.33±0.33	−0.09±0.61
V1504T/IIS4$_N$	−14.0±0.9 (5)	5.4±0.6	0.41±0.38	−0.54±0.64
GAGA+2 mutations				
L434T	−27.6±0.8 (6)	6.1±0.7	−0.71±0.44	
L434V	−30.2±0.7 (6)	6.3±0.6	−0.87±0.41	
A782P	−43.0±0.9 (6)	6.7±0.8	−1.81±0.55	
V1195T[c]	−28.9±0.7 (7)	5.1±0.7	−1.37±0.55	
I1505P	−8.7±0.8 (5)	5.5±0.6	0.99±0.34	
L434T/IIS4$_N$	−27.4±0.8 (6)	6.4±0.7	−0.57±0.42	−0.25±0.71
L434V/IIS4$_N$	−30.6±0.8 (6)	6.8±0.6	−0.69±0.39	−0.22±0.68
A782P/IIS4$_N$	−50.2±0.8 (5)	7.4±0.6	−2.00±0.45	−0.58±0.80
V1195T/IIS4$_N$	−25.3±1.0 (6)	4.5±0.8	−1.28±0.66	−0.30±0.94
I1505P/IIS4$_N$	−7.5±0.9 (5)	5.1±0.8	1.06±0.36	−0.32±0.61

Numbers of experiments are indicated in parentheses

*p<0.05, statistically significantly different from 0

[a] No currents could be measured if the charges in segments IS4 (IS4$_N$), IIIS4 (IIIS4$_N$) and IVS4 (IVS4$_N$) were replaced by glutamines

[b] Data from Depil et al. [10]

[c] Data from Beyl et al. [2]

investigated by means of mutant cycle analysis. This approach enables the estimation of interaction energies between the mutated pore residues in segments IS6–IVS6 and the voltage sensor in domain II (IIS4) on the basis of the
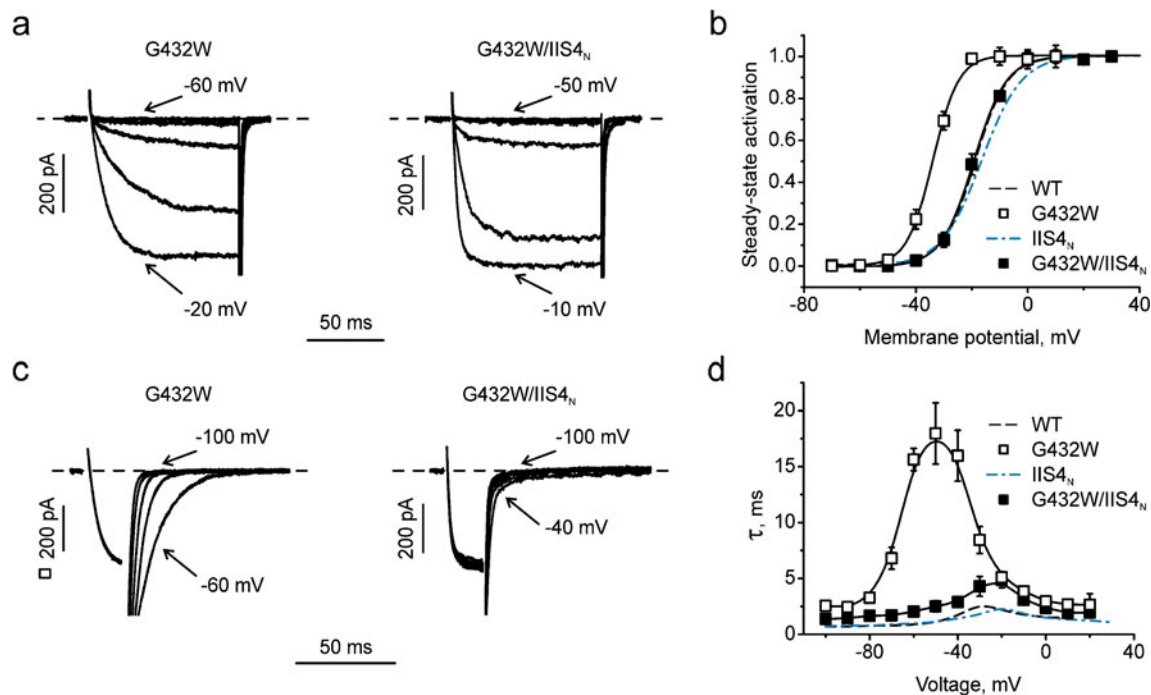
Fig. 2 Charge neutralisation in IIS4 rescues a gating disturbances induced by G432W in segment IS6. **a, c** Representative activation (**a**) and tail currents (**c**) traces through G432W and G432W/IIS4$_N$ mutant channels. **b, d** Averaged activation curves (**b**) and voltage dependence of the activation/deactivation time constants (**d**) of WT, G432W, IIS4$_N$ and G432W/IIS4N

free energy changes [18, 33, 51, 54]. The interaction energies were estimated by calculating the free energies as described in Kudrnac et al. [24] according to $\Delta G_{mut} = RT \left(\frac{V_{0.5,mut}}{k_{mut}} - \frac{V_{0.5,wt}}{k_{wt}} \right)$, $\Delta G_{IIS4} = RT \left(\frac{V_{0.5,IIS4}}{k_{IIS4}} - \frac{V_{0.5,wt}}{k_{wt}} \right)$ $\Delta G_{mut/IIS4} = RT \left(\frac{V_{0.5,mut/IIS4}}{k_{mut/IIS4}} - \frac{V_{0.5,wt}}{k_{wt}} \right)$ and $\Delta\Delta G = \Delta G_{mut/IIS4} - \Delta G_{mut} - \Delta G_{IIS4}$, with $V_{0.5}$ representing the voltage of steady-state (equilibrium) half-activation and k the slope factor (Table 1).

If the residues in segments IS6–IVS6 do not interact with the IIS4$_N$ segment, then the change in free energy ($\Delta G_{mut/IIS4}$) of the combined construct should be equal to the sum of the changes in free energy (ΔG_{mut} and ΔG_{IIS4}). If the residues are energetically coupled, then the change in free energy for the combination mutant would be significantly different from the sum of the two separate mutations.

Our data show that mutations in positions G432 (IS6), G1193 (IIIS6) and A1503 (VIS6) are energetically coupled with segment IIS4. This is evident from the non-additive shifts of the activation curves of the combined constructs (S6$_{mut}$/IIS4$_N$), which strongly suggest interdependence of the gating perturbations in IIS4 and the S6 residues (e.g. $\Delta\Delta G = 3.68 \pm 0.90$ kcal/mol for G1193T/IIS4$_N$, see also Table 1). Analysis of the other combined constructs shows that mutations in IIS4 do not interact with a series of other mutations in IS6, IIIS6 or IVS6 (GAGA−1, GAGA+1 or GAGA+2), with $\Delta\Delta G \approx 0$ kcal/mol. We therefore conclude that the conformational changes in the voltage sensor IIS4 and the S6 residues outside

the GAGA ring are energetically independent. While $\Delta\Delta G$ of construct A780T/IIS4$_N$ was not significantly different from 0 ($\Delta\Delta G = 0.96 \pm 0.99$ kcal/mol), the next residue downstream I781T was found to be energetically coupled to IIS4$_N$ ($\Delta\Delta G$ of I781T/IIS4$_N = -1.44 \pm 0.74$ kcal/mol, Table 1).

Discussion

If we translate the Hodgkin–Huxley model for potassium currents into current terminology, we can say that all four gating units (S4 segments) must be in an activated position before the channel can open [19]. This hypothesis was supported by Horn et al. [21] showing that immobilisation of only one S4 segment in its down position prevents *Shaker* activation. Interestingly, potassium channel closure (deactivation) seems to require only one S4 in its resting position [13, see also 23]. Here we demonstrate that a single voltage sensor (IIS4) in an asymmetric Ca$_V$1.2 interacts with a ring of conserved small residues (GAGA ring) in all four S6 segments.

Figure 1 illustrates that charge neutralisation of IIS4 (replacing residues R1–R5 by glutamines, IIS4$_N$) has no detectable effects on channel kinetics. In order to resolve potential IIS4$_N$ effects on current kinetics, we combined these mutations with S6 gating perturbations inducing pronounced shifts of the activation curve. In part, we utilised previously studied Ca$_V$ mutations (see [3, 10, 20, 24, 35, 48]) inducing $\Delta V > 10$ mV regardless of the physicochemical
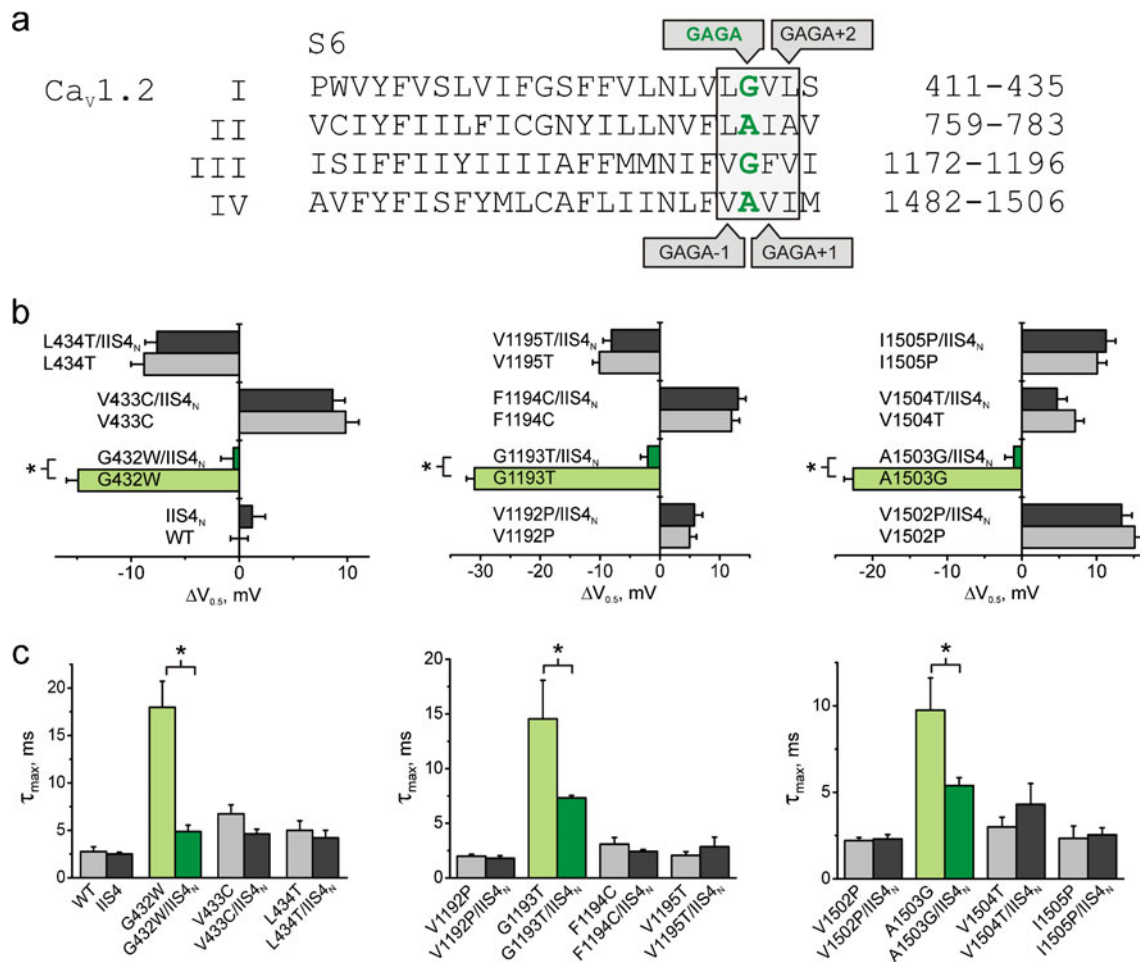
Fig. 3 Charge neutralisation in domain II (IIS4) rescues gating disturbances in GAGA positions of domains I, III and IV. **a** Alignment of S6 segments of Ca$_V$1.2 (accession number, P15381). The "GAGA" ring of small conserved residues in IS6–IVS6 is highlighted in *green*. Mutated residues are *boxed*. **b, c** Shift of activation curve (**b**) and peak activation/deactivation time constants (**c**) of the studied pore mutations in segments IS6 (*left*), IIIS6 (*middle*) and IVS6 (*right*) either alone or in combination with IIS4$_N$. Statistically significantly different (*t* test) values are marked with *asterisks*. *Error bars* indicate SEM

properties of the substituent (see marks and subscripts to Table 1). The resulting S6$_{mut}$/IIS4$_N$ constructs emerged as tools to analyse voltage sensor/S6 interactions.

IIS4 interactions with segments IS6–IVS6

As shown in Figs. 2, 3 and 4, combining IIS4$_N$ with mutations in the gating-sensitive regions of pore-forming S6 segments produced three kinetic phenotypes. First, four of the S6 mutants (G432W (IS6), G1193T (IIIS6), A1503G (VIS6) and partially A780T (IIS6)) were rescued by IIS4$_N$ (coloured bars on Figs. 3 and 4, Supplemental Fig. 1). This is evident from the unexpected backwards shifts of the activation curves towards wild type (Fig. 3b) and accompanying acceleration of channel kinetics (Fig. 3c). Thermodynamic cycle analysis supports the hypothesis that IIS4 interacts with GAGA residues (e.g. $\Delta\Delta G$(G432W/IIS4$_N$)= 1.84±0.72 kcal/mol, $\Delta\Delta G$(G432N/IIS4$_N$)=1.43±0.65 kcal/

mol, $\Delta\Delta G$(G1193T/IIS4$_N$)=3.68±0.90 kcal/mol and $\Delta\Delta G$ (A1503G/IIS4$_N$)=2.22±0.70 kcal/mol, see Table 1). Interestingly, the rightward shift of the activation curve in A780T/IIS4$_N$ was less pronounced (Fig. 4a, left column) and $\Delta\Delta G$ not significantly different from zero (Table 1). We speculate that these peculiarities are caused by domain-specific interactions between IIS4 and IIS6 (see detailed discussion below).

Second, pore mutants in segments IS6, IIIS6 and IVS6 upstream and downstream of the GAGA ring (see Fig. 3a) were not significantly affected by charge neutralisation in IIS4 (Fig. 3b, c; Supplemental Fig. 1). The effect of IIS4$_N$ in these constructs was comparable to the one observed for wild type (IIS4$_N$, Fig. 1). Additional experiments were carried out to analyse a potential "mutation dependence" of the position-specific rescue effect. As illustrated in Fig. 1 (in Supplemental Material), only substitution G432N in segment IS6 was rescued (G432N/IIS4$_N$, green bars,
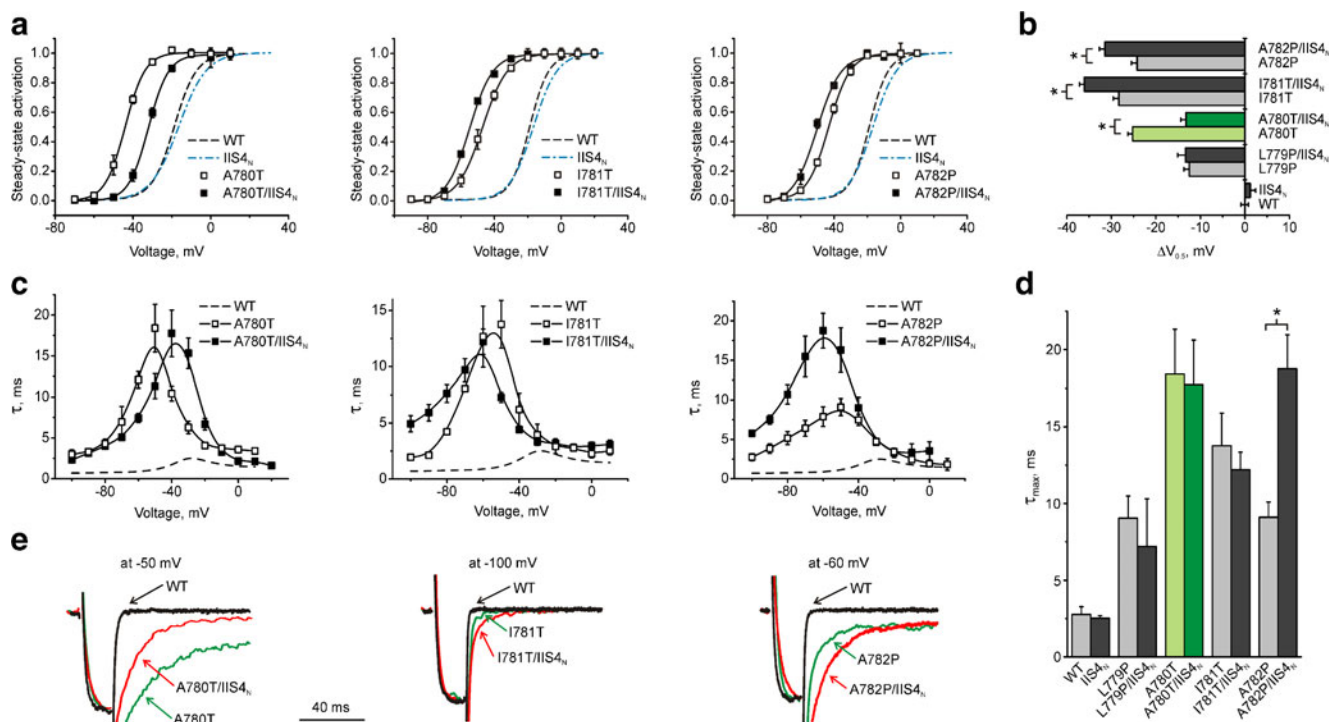
Fig. 4 Interaction of IIS4 with IIS6. **a** Averaged activation curves of WT ($n=9$), IIS4$_N$ ($n=11$) and mutations A780T (*left*), I781T (*middle*) and A782P (*right*) in domain II ($n=5$–10). **b** Shifts of the activation curves induced by IIS6 mutation (*light bars*) and in combination with IIS4$_N$ (*dark bars*). Statistically significant differences (unpaired t test) are marked with *asterisks*. **c** Voltage dependence of the activation/ deactivation time constants for indicated constructs. **d** Maximal activation/deactivation time constants of IIS6 mutations alone (*light bars*) and in combination with IIS4$_N$ (*dark bars*). **e** Selected tail currents through WT, A780T and A780T/IIS4$_N$ mutant channels at the indicated voltages

Supplemental Fig. 1) while alternative mutations of neighbouring residues (L431V, V433L and L434V) were not sensitive to IIS4$_N$ (compare with similar findings in Fig. 3b, c).

Third, combining IIS4$_N$ with I781T and I782P augmented the gating disturbances as evident from the additional shift of the activation curve to the left (Fig. 4a) and deceleration of deactivation kinetics (Fig. 4c). If we envisage the voltage sensor predominantly "pushing" the gating structures of Ca$_V$1.2 into the closed conformation [2], then charge neutralisation of IIS4 would decelerate channel closure at negative voltages (i.e. slow deactivation). Such "expected gating changes" were observed only for constructs I781T/IIS4$_N$ and A782P/IIS4$_N$ (Fig. 4).
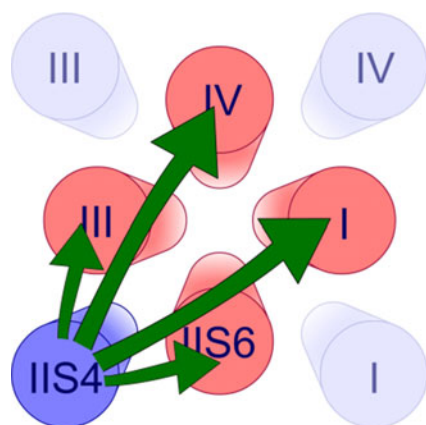
Scheme 1 Hypothetical long range interactions of segment IIS4 with all four S6 segments
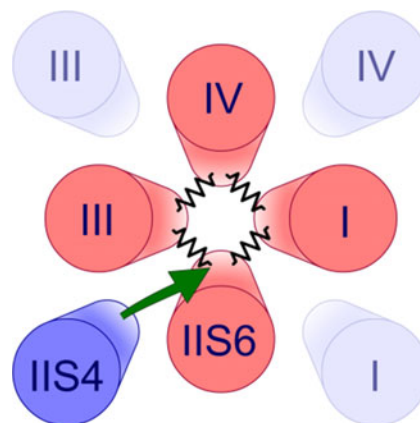
Scheme 2 Cooperative gating model: A single voltage sensor (IIS4) interacts with an S6 segment which facilitates the stabilisation of closed state formation by all four S6 segments

Dual role of A780?

Interestingly, the activation curve of A780T/IIS4$_N$ was shifted towards the wild type position, but only half way (Fig. 4a, left column). This distinguishes A780T from the other GAGA mutants. We speculate that IIS4$_N$ would potentially shift the activation curve of A780T/IIS4$_N$ to the right (Fig. 3b). A780 is, however, also part of the IIS6 gating structure where combinations with IIS4$_N$ induce leftward shifts (compare with other IIS6 mutants I781T and A782P, Fig. 4). Such opposing effects could explain an incomplete backward shift of the activation curve of A780T/IIS4$_N$ (Fig. 4a).

Conclusions and outlook

The principal finding of our study is that segment IIS4 interacts with a ring of conserved small residues in segments IS6–IVS6 (GAGA ring [10]). In general, the interaction of a single

voltage sensor with all four S6 (and associated gate structures) suggests either interactions of IIS4 with each of them (Scheme 1) or, alternatively, interactions with the gate structures in domain II that are cooperatively linked to other domains (Scheme 2).

The distances between the GAGA residues (corresponding to AAAA in the crystal structure of a homologous bacterial sodium channel Na$_V$Ab [29]) and the voltage sensor segments are illustrated in Fig. 5b. Such long range interactions between segment IIS4 and S6 residues in domains I, III and IV cannot be excluded but would have to occur via different distances (IIS4–IS6, 21 Å; IIS4–IIIS6, 40 Å and IIS4–IVS6, 36 Å) and different pathways in a highly specific manner.

We favour a "cooperative gating model" illustrated in Scheme 2. Cooperative interactions between individual amino acids of pore-forming S6 segments of Ca$_V$1.2 were previously identified [24]. Moreover, in the closed state, the small residues of the GAGA ring are apparently in tight contact with neighbouring bulky amino acids which may
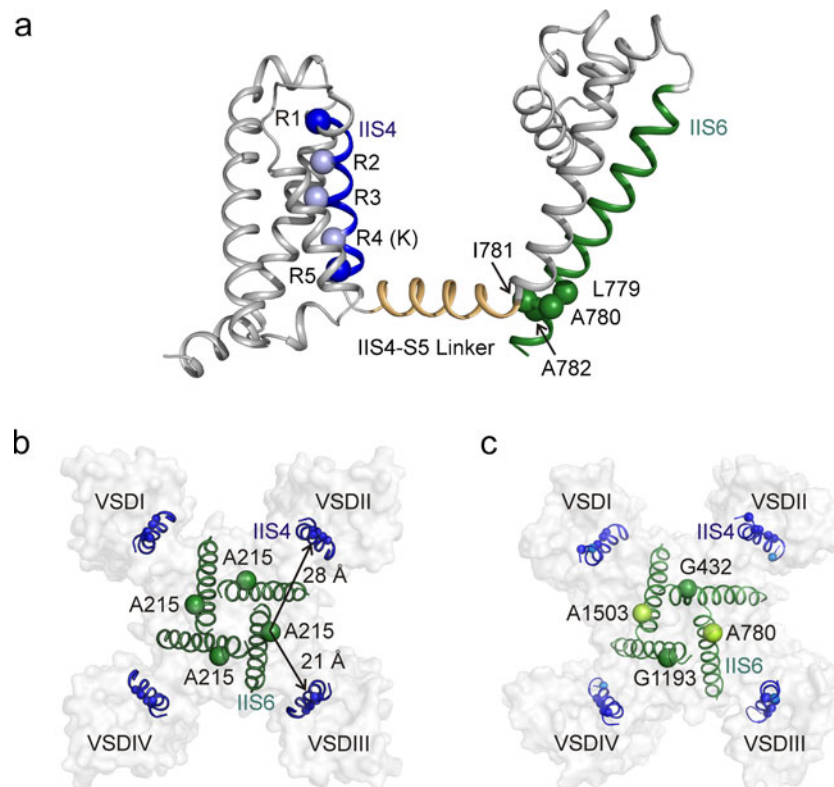

Fig. 5 Ca$_V$1.2 homology model based on Na$_V$Ab crystal structure [29] illustrates the location of the GAGA ring with respect to S4. **a** *Blue spheres* represent the arginine (R650, R653, R656 and R662) and lysine (K659) positions in segment IIS4. A previously identified gating-sensitive motif (LAIA [20]) in IIS6 is shown as *green spheres*. The linker helix is coloured *orange*. Figures generated with Pymol (The PyMOL Molecular Graphics System, Version 1.2r3pre, Schrödinger, LLC). In analogy to K$_V$ and Na$_V$ crystal structures, we speculate that in the closed conformation, LAIA residues [20] in the bundle crossing region of S6 interact with the voltage sensor domain via the

S4–S5 linker (e.g. I781 is in direct contact with the linker which would enable to force the IIS6 segment towards its closed position; see details in Discussion section on IIS4–IIS6 interaction). **b**, **c** Bottom view of the pore domain and S4 segments of Na$_V$Ab crystal structure and Ca$_V$1.2 homology model coloured as in panel A. The GAGA ring [10] (corresponding to AAAA ring in Na$_V$Ab) is shown as *green spheres*. The distances between the AAAA ring in the Na$_V$Ab crystal structure (corresponding to GAGA in Ca$_V$1.2) with respect to the voltage-sensing domains are indicated

stabilise the closed channel state [10]. Channel closure is initiated by downward movement of an S4 segment and subsequent translocation of the corresponding S6 towards the resting position via the S4–S5 linkers (Fig. 5a). In its closing position, a single S6 segment is stabilised by cooperative interactions (e.g. hydrophobic) with gate structures of neighbouring domains (see [3]). In other words, a single S6 segment in its closing position increases the probability of closed state formation by all four S6 segments. The effect that only conformational changes in the GAGA positions are reversed by charge neutralisation in IIS4 warrants further research.

We speculate that in $Ca_V1.2$ (in analogy to K_V) any single S4 segment may initiate channel closure under hyperpolarizing voltage [13]. To enable channel opening, however, all four S4 segments must be activated [21]. Phillips and Swartz [31] have shown that K_V opens while S4 segments are still moving (i.e. they do not reach their fully activated position). We therefore further speculate that opening of $Ca_V1.2$ occurs when all four S4 segment left the resting state.

In wild type $Ca_V1.2$, S6 segments form a tight closed conformation, with the GAGA ring playing a key role. Hence, substitution of any of the GAGA residues by a bulky tryptophan (G432W), polar threonine (A780T) or a helix-bending proline (A780P) disturbs the fine-tuned closure mechanism, as is evident from the slow deactivation. Such a slowing of S6 gating would affect the corresponding S4 transitions to the resting state. Correspondingly, translocation of all S4 segments in their resting position interferes with the pore closure of the mutants. In such a scenario, removal of a "disturbing IIS4 interaction" with the cooperative GAGA ring might relieve spatial constraints thereby providing more flexibility for pore-closing interactions [3]. Cooperative interactions are not restricted to interactions within the GAGA ring. Contributions of residues in segments IS6 and IIS6 to activation gating in $Ca_V1.2$ have previously been demonstrated for Ser-435 (IS6) and Ile-781 (IIS6) [24], suggesting that paired interactions between additional S6 gating structures may stabilise the closed state.

Replacing charged residues in segments IS4–IVS4 with neutral glutamines resulted in only one functional construct ($IIS4_N$, Table 1) which warrants further research. Interestingly, Gagnon and Bezanilla [13] observed substantial reduction of the current amplitudes if the charged residues of S4 segments in a symetric potassium channel concatemer were subsequently substituted by glutamine or asparagine, suggesting that neutralisation of charged residues in S4 segments my affect expression density, membrane targeting or the functionality of these constructs.

References

1. Armstrong CM, Bezanilla F (1973) Currents related to movement of the gating particles of the sodium channels. Nature 242:459–461
2. Beyl S, Kügler P, Kudrnac M, Hohaus A, Hering S, Timin E (2009) Different pathways for activation and deactivation in $Ca_V1.2$: a minimal gating model. J Gen Physiol 134:231–241
3. Beyl S, Depil K, Hohaus A, Stary-Weinzinger A, Timin E, Shabbir W, Kudrnac M, Hering S (2011) Physicochemical properties of pore residues predict activation gating of $Ca_V1.2$: a correlation mutation analysis. Pflugers Arch 461:53–63
4. Bezanilla F (2000) The voltage sensor in voltage-dependent ion channels. Physiol Rev 80:555–592
5. Bezanilla F, Perozo E, Stefani E (1994) Gating of Shaker K+ channels: II. The components of gating currents and a model of channel activation. Biophys J 66:1011–1021
6. Catterall WA (2000) Structure and regulation of voltage-gated Ca2+ channels. Annu Rev Cell Dev Biol 16:521–555
7. Catterall WA (2010) Ion channel voltage sensors: structure, function, and pathophysiology. Neuron 67:915–928
8. Catterall WA, Striessnig J, Snutch TP, Perez-Reyes E (2003) International Union of Pharmacology. XL. Compendium of voltage-gated ion channels: calcium channels. Pharmacol Rev 55:579–581
9. Del Camino D, Kanevsky M, Yellen G (2005) Status of the intracellular gate in the activated-not-open state of Shaker K+ channels. J Gen Physiol 126:419–428
10. Depil K, Beyl S, Stary-Weinzinger A, Hohaus A, Timin E, Hering S (2011) Timothy mutation disrupts the link between activation and inactivation in Ca(V)1.2 protein. J Biol Chem 286:31557–31564
11. Ellis SB, Williams ME, Ways NR, Brenner R, Sharp AH, Leung AT, Campbell KP, McKenna E, Koch WJ, Hui A (1988) Sequence and expression of mRNAs encoding the alpha 1 and alpha 2 subunits of a DHP-sensitive calcium channel. Science 241:1661–1664
12. Eswar N, Webb B, Marti-Renom MA, Madhusudhan MS, Eramian D, Shen M-Y, Pieper U, Sali A (2006) Comparative protein structure modeling using Modeller. Curr Protoc Bioinformatics Chapter 5, Unit 5.6
13. Gagnon DG, Bezanilla F (2009) A single charged voltage sensor is capable of gating the Shaker K+ channel. J Gen Physiol 133:467–483
14. Hackos DH, Chang T-H, Swartz KJ (2002) Scanning the intracellular S6 activation gate in the shaker K+ channel. J Gen Physiol 119:521–532
15. Hamill OP, Marty A, Neher E, Sakmann B, Sigworth FJ (1981) Improved patch-clamp techniques for high-resolution current recording from cells and cell-free membrane patches. Pflugers Arch 391:85–100
16. Hemara-Wahanui A, Berjukow S, Hope CI, Dearden PK, Wu S-B, Wilson-Wheeler J, Sharp DM, Lundon-Treweek P, Clover GM, Hoda J-C, Striessnig J, Marksteiner R, Hering S, Maw MA (2005) A CACNA1F mutation identified in an X-linked retinal disorder shifts the voltage dependence of $Ca_V1.4$ channel activation. Proc Natl Acad Sci U S A 102:7553–7558
17. Hering S (2002) Beta-subunits: fine tuning of Ca(2+) channel block. Trends Pharmacol Sci 23:509–513
18. Hidalgo P, MacKinnon R (1995) Revealing the architecture of a K + channel pore through mutant cycles with a peptide inhibitor. Science 268:307–310
19. Hodgkin AL, Huxley AF (1952) A quantitative description of membrane current and its application to conduction and excitation in nerve. J Physiol Lond 117:500–544

20. Hohaus A, Beyl S, Kudrnac M, Berjukow S, Timin EN, Marksteiner R, Maw MA, Hering S (2005) Structural determinants of L-type channel activation in segment IIS6 revealed by a retinal disorder. J Biol Chem 280:38471–38477

21. Horn R, Ding S, Gruber HJ (2000) Immobilizing the moving parts of voltage-gated ion channels. J Gen Physiol 116:461–476

22. Hoshi T, Zagotta WN, Aldrich RW (1994) Shaker potassium channel gating. I: transitions near the open state. J Gen Physiol 103:249–278

23. Jensen MØ, Jogini V, Borhani DW, Leffler AE, Dror RO, Shaw DE (2012) Mechanism of voltage gating in potassium channels. Science 336:229–233

24. Kudrnac M, Beyl S, Hohaus A, Stary A, Peterbauer T, Timin E, Hering S (2009) Coupled and independent contributions of residues in IS6 and IIS6 to activation gating of CaV1.2. J Biol Chem 284:12276–12284

25. Ledwell JL, Aldrich RW (1999) Mutations in the S4 region isolate the final voltage-dependent cooperative step in potassium channel activation. J Gen Physiol 113:389–414

26. Long SB, Campbell EB, Mackinnon R (2005) Crystal structure of a mammalian voltage-dependent Shaker family K+ channel. Science 309:897–903

27. Murata Y, Iwasaki H, Sasaki M, Inaba K, Okamura Y (2005) Phosphoinositide phosphatase activity coupled to an intrinsic voltage sensor. Nature 435:1239–1243

28. Pathak M, Kurtz L, Tombola F, Isacoff E (2005) The cooperative voltage sensor motion that gates a potassium channel. J Gen Physiol 125:57–69

29. Payandeh J, Scheuer T, Zheng N, Catterall WA (2011) The crystal structure of a voltage-gated sodium channel. Nature 475:353–358

30. Perez-Reyes E, Castellano A, Kim HS, Bertrand P, Baggstrom E, Lacerda AE, Wei XY, Birnbaumer L (1992) Cloning and expression of a cardiac/brain beta subunit of the L-type calcium channel. J Biol Chem 267:1792–1797

31. Phillips LR, Swartz KJ (2010) Position and motions of the S4 helix during opening of the Shaker potassium channel. J Gen Physiol 136:629–644

32. Ramsey IS, Moran MM, Chong JA, Clapham DE (2006) A voltage-gated proton-selective channel lacking the pore domain. Nature 440:1213–1216

33. Ranganathan R, Lewis JH, MacKinnon R (1996) Spatial localization of the K+ channel selectivity filter by mutant cycle-based structure analysis. Neuron 16:131–139

34. Raybaud A, Dodier Y, Bissonnette P, Simoes M, Bichet DG, Sauvé R, Parent L (2006) The role of the GX9GX3G motif in the gating of high voltage-activated Ca2+ channels. J Biol Chem 281:39424–39436

35. Raybaud A, Baspinar E-E, Dionne F, Dodier Y, Sauvé R, Parent L (2007) The role of distal S6 hydrophobic residues in the voltage-dependent gating of CaV2.3 channels. J Biol Chem 282:27944–27952

36. Sasaki M, Takagi M, Okamura Y (2006) A voltage sensor-domain protein is a voltage-gated proton channel. Science 312:589–592

37. Schoppa NE, Sigworth FJ (1998) Activation of Shaker potassium channels I. Characterization of voltage-dependent transitions. J Gen Physiol 111:271–294

38. Schoppa NE, Sigworth FJ (1998) Activation of Shaker potassium channels II. Kinetics of the V2 mutant channel. J Gen Physiol 111:295–311

39. Schoppa NE, Sigworth FJ (1998) Activation of Shaker potassium channels III. An activation gating model for wild-type and V2 mutant channels. J Gen Physiol 111:313–342

40. Smith-Maxwell CJ, Ledwell JL, Aldrich RW (1998) Role of the S4 in cooperativity of voltage-dependent potassium channel activation. J Gen Physiol 111:399–420

41. Smith-Maxwell CJ, Ledwell JL, Aldrich RW (1998) Uncharged S4 residues and cooperativity in voltage-dependent potassium channel activation. J Gen Physiol 111:421–439

42. Splawski I, Timothy KW, Sharpe LM, Decher N, Kumar P, Bloise R, Napolitano C, Schwartz PJ, Joseph RM, Condouris K, Tager-Flusberg H, Priori SG, Sanguinetti MC, Keating MT (2004) Ca (V)1.2 calcium channel dysfunction causes a multisystem disorder including arrhythmia and autism. Cell 119:19–31

43. Splawski I, Timothy KW, Decher N, Kumar P, Sachse FB, Beggs AH, Sanguinetti MC, Keating MT (2005) Severe arrhythmia disorder caused by cardiac L-type calcium channel mutations. Proc Natl Acad Sci USA 102(Keating MT):8089–8096, discussion 8086–8088

44. Stary A, Shafrir Y, Hering S, Wolschann P, Guy HR (2008) Structural model of the CaV 1.2 pore. Channels Austin 2:210–215

45. Stefani E, Toro L, Perozo E, Bezanilla F (1994) Gating of Shaker K+ channels: I. Ionic and gating currents. Biophys J 66:996–1010

46. Striessnig J, Bolz HJ, Koschak A (2010) Channelopathies in CaV1.1, CaV1.3, and CaV1.4 voltage-gated L-type Ca2+ channels. Pflugers Arch 460:361–374

47. Sukhareva M, Hackos DH, Swartz KJ (2003) Constitutive activation of the Shaker KV channel. J Gen Physiol 122:541–556

48. Tadross MR, Ben Johny M, Yue DT (2010) Molecular endpoints of Ca2+/calmodulin- and voltage-dependent inactivation of Ca (v)1.3 channels. J Gen Physiol 135:197–215

49. Talavera K, Nilius B (2006) Evidence for common structural determinants of activation and inactivation in T-type Ca2+ channels. Pflugers Arch 453:189–201

50. Wall-Lacelle S, Hossain MI, Sauvé R, Blunck R, Parent L (2011) Double mutant cycle analysis identified a critical leucine residue in the IIS4S5 linker for the activation of the Ca(V)2.3 calcium channel. J Biol Chem 286:27197–27205

51. Yifrach O, MacKinnon R (2002) Energetics of pore opening in a voltage-gated K(+) channel. Cell 111:231–239

52. Zagotta WN, Hoshi T, Aldrich RW (1994) Shaker potassium channel gating. III: evaluation of kinetic models for activation. J Gen Physiol 103:321–362

53. Zagotta WN, Hoshi T, Dittman J, Aldrich RW (1994) Shaker potassium channel gating. II: transitions in the activation pathway. J Gen Physiol 103:279–319

54. Zandany N, Ovadia M, Orr I, Yifrach O (2008) Direct analysis of cooperativity in multisubunit allosteric proteins. Proc Natl Acad Sci U S A 105:11697–11702

55. Zhao Y, Scheuer T, Catterall WA (2004) Reversed voltage-dependent gating of a bacterial sodium channel with proline substitutions in the S6 transmembrane segment. Proc Natl Acad Sci U S A 101:17873–17878

56. Zhao Y, Yarov-Yarovoy V, Scheuer T, Catterall WA (2004) A gating hinge in Na+ channels; a molecular switch for electrical signaling. Neuron 41:859–865

57. Zhen X-G, Xie C, Fitzmaurice A, Schoonover CE, Orenstein ET, Yang J (2005) Functional architecture of the inner pore of a voltage-gated Ca2+ channel. J Gen Physiol 126:193–204